

# Three dimensional porous Cu-Zn/Al foam monolithic catalyst for CO<sub>2</sub> hydrogenation to methanol in microreactor



Zhuangdian Liang<sup>a,b,c,1</sup>, Peng Gao<sup>a,1</sup>, Zhiyong Tang<sup>a</sup>, Min Lv<sup>a,\*</sup>, Yuhua Sun<sup>a,c,\*\*</sup>

<sup>a</sup> CAS Key Lab of Low-Carbon Conversion Science and Engineering, Shanghai Advanced Research Institute, Chinese Academy of Sciences, No. 99 Hailue Road, Zhangjiang Hi-Tech Park, Shanghai 201210, China

<sup>b</sup> University of the Chinese Academy of Sciences, Beijing 100049, China

<sup>c</sup> School of Physical Science and Technology, ShanghaiTech University, Shanghai 201210, China

## ARTICLE INFO

### Keywords:

Carbon dioxide hydrogenation  
Copper-based catalyst  
Methanol synthesis  
Monolithic catalyst  
Microreactor

## ABSTRACT

CO<sub>2</sub> hydrogenation turns to be an attractive pathway of C1 conversion. For CO<sub>2</sub> hydrogenation to methanol, a novel method was investigated for the preparation of layer structured Cu-Zn/Al foam monolithic catalyst integrated with microreactor. Such a monolithic catalyst could be loaded in a flange-type microreactor in the form of packed bed to intensify the process. As a result, a high copper time yield of methanol, 7.81 g g<sub>Cu</sub><sup>-1</sup> h<sup>-1</sup>, was obtained at 250 °C, 3 MPa and 20000 mL g<sub>cat</sub><sup>-1</sup> h<sup>-1</sup> due to the heat/mass-transfer properties with microreactor. Besides, the monolithic catalyst showed a good ability of adhesion.

## 1. Introduction

Recently, conversion of CO<sub>2</sub> to methanol is considered as an effective way for CO<sub>2</sub> utilization. Both as a green liquid fuel and as a feedstock of many value-added products, methanol plays an increasingly important role in chemical industry [1,2]. The utilization of CO<sub>2</sub> as a feedstock for producing chemicals is an effective method to relieve climate changes caused by increasing CO<sub>2</sub> in the atmosphere, as well as providing a great opportunity in developing new concepts for catalysts and industrial process [3]. Methanol synthesis from CO<sub>2</sub> hydrogenation with the aid of renewable or low-carbon energy sources has already shown industrial viability [4,5].

As a highly exothermic reaction, CO<sub>2</sub> hydrogenation reaction is strongly influenced by the thermal management at the device level. Accumulation of reaction heat will increase the local temperature on the catalyst particle surface as well as the overall temperature of the reaction system, which will consequently lower methanol selectivity, promote side reactions, cause catalyst sintering and degradation [6,7]. Furthermore, other by-products are formed during the hydrogenation of CO<sub>2</sub>, such as CO, hydrocarbons, and higher alcohols [8]. Therefore, a highly selective catalyst is required to avoid the formation of undesired byproducts for methanol synthesis. In addition, meso- and macro-pores in catalyst substrate can effectively promote heat and mass transport to intensify progress [9,10]. Tubular fixed bed reactor is commonly used

for CO<sub>2</sub> hydrogenation to methanol synthesis. Due to the limitation of heat transfer in fixed bed reactor, it is always challenging to avoid the hotspot and temperature runaway.

The process intensification potential of microreactor has attracted attention in the field of energy technology. The specific features of microreactor mainly include: (1) enhanced heat and mass transfer, (2) narrow residence time distributions due to fast species exchange by diffusion in the small lateral dimensions, and (3) low pressure drop. Therefore, it is a particularly interesting choice for those gas conversion processes in which selectivity and conversion are closely related to the heat/mass transfer properties of reactor and catalyst. However, most existing methods of combining catalyst and microreactor are often constrained to certain disadvantages such as easily crushed layer for washcoating, hotspot and sintering for catalyst particles in fixed bed. Hence, the distinctive feature of heat and mass transfer ability of microreactor could be hindered by directly filling catalyst particles into microchannel [11].

In our previous work, Cu-Zn-Al layer structure compounds were selected as the precursors [12–15]. Small Cu clusters were generated as the active sites for CO<sub>2</sub> hydrogenation to methanol. The Cu-Zn-Al catalyst was synthesized through co-precipitation methods. The atomic level homogeneous dispersion of catalyst brought high stability and activity. In addition, catalyst particles were diluted with quartz sand and then tested in the fixed bed reactor [16]. A good catalytic

\* Corresponding author.

\*\* Corresponding author at: CAS Key Lab of Low-Carbon Conversion Science and Engineering, Shanghai Advanced Research Institute, Chinese Academy of Sciences, No. 99 Hailue Road, Zhangjiang Hi-Tech Park, Shanghai 201210, China.

E-mail addresses: lvm@shar.ac.cn (M. Lv), sunyh@sari.ac.cn (Y. Sun).

<sup>1</sup> Contributed equally to this work.

performance of 25% CO<sub>2</sub> conversion and 60% methanol selectivity was achieved [17].

Moreover, hydrothermal synthesis is an alternative process to make layered materials. Layer structure compounds on Al substrate can be synthesized via hydrothermal approach, which employs the Al substrate of a trivalent metal instead of its salt and oxide to be catalyst substrate. It has been proved that the monolithic catalyst supported by metal foam presents better performance than the particle catalyst for an exothermic reaction [18]. Monolithic catalyst in microreactor effectively minimizes sintering and stabilizes the coke formation [19,20].

The focus of this paper is to study the new method of preparing monolithic catalyst of CO<sub>2</sub> hydrogenation to methanol and investigate the influence of reaction condition on catalytic performance in microreactor. By efficiently integrating catalyst with microreactor, this method is helpful to fix the most critical problem of microreactor [21,22]. The textural and structural properties of monolithic catalyst were characterized in detail. And the advantage of this method to prepare the catalyst used in microreactor was discussed.

## 2. Experimental section

### 2.1. Aluminum foam as catalyst support

**Fig. 1A(a)** shows the photograph of three dimensional porous aluminum foams (Suzhou Jiashide Metal Foam Co., Ltd., China) used in the present work with 120 Pores Per Linear Inch (PPI). Each block of aluminum foam was sized into 20 × 50 × 1 mm. Aluminum foam not only has meso- and macro-pores in the three dimensional porous structure, but also shows a good property in heat transfer by inheriting

metallic characteristics. Prior to the experiment, the aluminum form was degreased in acetone with consecutively ultrasonic shaking for 5 min. Then, the aluminum form was etched with 0.4 mol L<sup>-1</sup> HCl for 10 min at room temperature. After rinsed with water and consecutively ultrasonic shaking for 10 min, the aluminum support for catalyst preparation was obtained.

### 2.2. Catalyst preparation

In this study, layer structure attached on aluminum support named Cu-Zn/Al foam was prepared via a hydrothermal method. In a typical procedure to synthesize hydrotalcite nanostructure, 100 mL solution of cupric oxalate (CuC<sub>2</sub>O<sub>4</sub>, 24 mmol L<sup>-1</sup>) and zinc acetate (Zn (CH<sub>3</sub>COO)<sub>2</sub>, 46 mmol L<sup>-1</sup>) was magnetically stirred for 2 h at room temperature. The pH of the solution is approximately 7 detected by pH indicator strips. The obtained solution was transferred into autoclave and ready for the growth of nanostructure. Afterwards, the pre-treated aluminum foam was immersed into the reaction solution. Then the autoclave was sealed and rotated at the rate of 20 r min<sup>-1</sup> which lasted 24 h at 70 °C for hydrothermal nanostructure growth. After hydrothermal procedure, the autoclave was cooled down to ambient temperature. Dark brown monolithic precursors were taken out and rinsed with distilled water several times. After that, the sample was calcined in the atmosphere at 350 °C for 4 h.

### 2.3. Characterization

The morphology of the monolithic catalysts was investigated in a ZEISS SUPRA 55 scanning electron microscope (SEM) at 2.00 kV

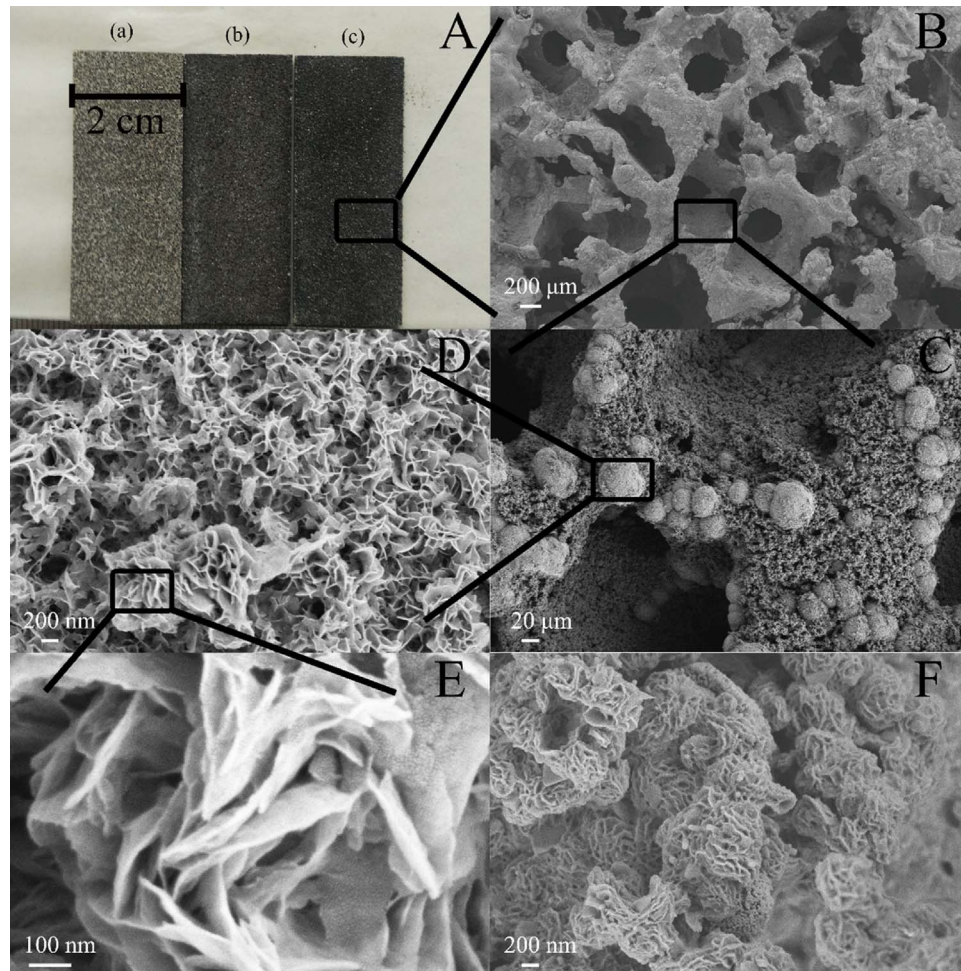


**Fig. 1.** All-in-one for the monolithic catalysts. A: Photograph of the macroscopic sample, (a) the Al foam (b) the catalyst after hydrothermal method (c) the catalyst of Cu-Zn/Al foam after calcine; B-E: SEM image in different magnifications, showing the three dimensional porous structure and surface morphology of monolithic catalysts; F: SEM image of spent monolithic catalysts.

acceleration voltage. The catalyst foam was carved into a cube (about 10 mm squared), and element distribution on the catalyst surface was detected by Energy Dispersive Spectrometer (EDS) of Oxford Instruments 10 mm<sup>2</sup> SDD detector x-act.

The specific area of the monolithic catalysts was measured by Nitrogen Adsorption. In pretreatment, about 200 mg sample was degassed at 200 °C in vacuum for 12 h. Afterwards, the sample was tested at –196 °C in a Micromeritics TriStar 3020 instrument. The specific surface area was determined by the Brunauer–Emmett–Teller (BET) method. The obtainment of pore volume and the pore size were based on the Barrett–Joyner–Halenda (BJH) method.

The actual amount of metal loaded in the monolithic catalysts was analyzed in PerkinElmer Optima 8000 inductive coupled plasma emission spectrometer (ICP) by completely dissolving 200 mg samples in a warm HNO<sub>3</sub> solution.

The crystal phase composition of the monolithic catalysts was detected by X-ray diffraction (XRD) measurement that was recorded on a Rigaku Ultima 4 X-ray diffractometer. The samples were tested under radiation of Cu Kα with scanning angle from 10° to 90° and rate of 4° min<sup>−1</sup>, the calcined samples were measured at room temperature.

The phase and composition of the monolithic catalysts were verified by X-ray photoelectron spectroscopy (XPS) that Al Kα ( $\text{h}\nu = 1486.6 \text{ eV}$ ) radiation was used on a Thermo Scientific K-Alpha spectrometer. The data were calibrated by the C 1s peak at 284.6 eV. Based on the sensitivity factor method, the surface metal contents of the samples were determined from the peak area of Cu 2p<sub>3/2</sub> and Zn 2p<sub>3/2</sub> [23].

The reducibility of the monolithic catalysts was measured in Micromeritics AutoChem 2920 instrument based on Temperature-Programmed Reduction (TPR). The sample was rinsed with helium at 120 °C. After cooled to 60 °C, the sample was reduced by H<sub>2</sub> with the temperature gradually increased to 500 °C at a heating rate of 10 °C min<sup>−1</sup>. The tail gas was analyzed by a thermal conductivity detector (TCD).

The basicity of monolithic catalysts was measured in Micromeritics AutoChem 2920 instrument based on Temperature-Programmed Desorption (TPD). Firstly, the sample was reduced by H<sub>2</sub> at 250 °C. Then it was cooled to room temperature and pure CO<sub>2</sub> entered for saturated adsorption. After rinsed with argon, the sample was heated at a temperature rate of 10 °C min<sup>−1</sup> under argon, and the desorbed CO<sub>2</sub> was detected by TCD [15].

The dispersion of copper ( $D_{\text{Cu}}$ ) was calculated by dissociative N<sub>2</sub>O adsorption on Micromeritics AutoChem 2920 instrument. The samples were reduced completely in H<sub>2</sub> at 250 °C, the hydrogen consumption was noted as  $X$ . Then, the exposed Cu<sup>0</sup> was oxidized to Cu<sup>+</sup> by N<sub>2</sub>O. After cooled to ambient temperature under argon, the sample was reduced by H<sub>2</sub>, the hydrogen consumption was noted as  $Y$ . The dispersion of Cu ( $D_{\text{Cu}}$ ) was calculated by Eq. (1) [24].

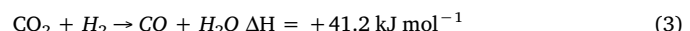
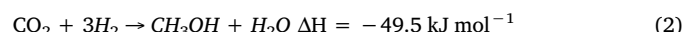
$$D_{\text{Cu}} = \frac{2Y}{X} \quad (1)$$

#### 2.4. Evaluation of catalysts

The test of CO<sub>2</sub> hydrogenation to methanol was carried out in a microreactor. The photographs of the reactor and experimental platform are shown in Fig. 2A and B. The reactor system was insulated by an insulation box with quartz visualization window (180 mm squared). The reactor was made by 316L stainless steel assembled plates. The exploded view of microreactor is illustrated in Fig. 2C. The chamber (depth: 2 mm; width: 20 mm; and length: 50 mm) for monolithic catalyst was milled on a 3 mm thick 316 L stainless steel rectangular plate (Fig. 2D). The reaction substrate plate was bolted between two cover plates. Three electrical heating rods were inserted into each cover plate. Temperature distribution was measured by three K-type thermocouples which are evenly placed in bottom cover plate. High-temperature

resistant gasket made of GARLAST was embedded between top cover and reaction plate to prevent leakage of gas during the reaction.

The catalyst was reduced in-situ with 10 vol% H<sub>2</sub>/N<sub>2</sub> with flow rate of 100 mL min<sup>−1</sup> at 250 °C for 5 h. After the reactor was cooled to 200 °C, gaseous mixture (volume fraction: H<sub>2</sub>/CO<sub>2</sub>/N<sub>2</sub> = 73/24/3) was fed into reactor. Then reactor was heated gradually to the reaction temperature. The flow rate of the gaseous mixture was monitored by a Brooks mass flow controller. The tail gas was online detected by gas chromatography (Agilent 7890B). Data were collected once the steady state was achieved and calculated by N<sub>2</sub> as the internal standard. The main reaction network of CO<sub>2</sub> hydrogenation includes the synthesis of methanol (Eq. (2)) and the reverse water-gas shift (RWGS) (Eq. (3)). Two chemical equations are as follows:



Based on the internal standard method, the CO<sub>2</sub> conversion ( $C_{\text{CO}_2}$ ) and selectivity product ( $S_a$ ) of chemical components (a) were calculated by the following Eqs. (4) and (5).

$$C_{\text{CO}_2} = \frac{F_{\text{in}}X_{\text{CO}_2} - F_{\text{out}}X_{\text{CO}_2,\text{out}}}{F_{\text{in}}X_{\text{CO}_2,\text{in}}} \times 100 = \left(1 - \frac{X_{\text{N}_2,\text{in}}X_{\text{CO}_2,\text{out}}}{X_{\text{N}_2,\text{out}}X_{\text{CO}_2,\text{in}}}\right) \times 100 \quad (4)$$

$$S_a = \frac{(F_{\text{out}}X_{(a)\text{out}} - F_{\text{in}}X_{(a)\text{in}}) \times n_{C(a)}}{F_{\text{in}}X_{\text{CO}_2,\text{in}} - F_{\text{out}}X_{\text{CO}_2,\text{out}}} \times 100 \quad (5)$$

In Eq. (4),  $F_{\text{in}}$  and  $F_{\text{out}}$  indicate the total flow rate at inlet and outlet of reactor;  $X_{\text{CO}_2,\text{in}}$  and  $X_{\text{CO}_2,\text{out}}$  indicate the concentration of CO<sub>2</sub> at inlet and outlet of reactor;  $X_{\text{N}_2,\text{in}}$  and  $X_{\text{N}_2,\text{out}}$  indicate the concentration of N<sub>2</sub> at inlet and outlet of reactor. In Eq. (5),  $X_{(a)\text{in}}$  and  $X_{(a)\text{out}}$  indicate the concentration of the components (a) at inlet and outlet of reactor. And  $n_{C(a)}$  indicates the number of carbon atom in molecular formula.

The copper time yield of methanol, noted as CH<sub>3</sub>OH Yield, which give the amount of CH<sub>3</sub>OH produced per gram of copper per hour, was defined by Eq. (6).

$$\text{The CH}_3\text{OH Yield} = \frac{\text{WHSV}}{22.4} \times C_{\text{CO}_2} \times S_{\text{methanol}} \times \frac{M_{\text{methanol}}}{W_{\text{Cu}}} \quad (6)$$

In this equation, WHSV is the weight hourly space velocity of feed gas (L g<sub>cat</sub><sup>−1</sup> h<sup>−1</sup>);  $C_{\text{CO}_2}$  is the conversion of CO<sub>2</sub>;  $S_{\text{methanol}}$  is the selectivity of methanol;  $M_{\text{methanol}}$  is the molecular weight of methanol;  $W_{\text{Cu}}$  is the weight of Cu (g) in the catalyst per gram.

### 3. Results and discussion

#### 3.1. Characterization

##### 3.1.1. Textural and structural properties of the Cu-Zn/Al foam monolithic catalyst

The typical micrograph of layer structure is illustrated in Fig. 1B–F [25]. Fig. 1B clearly shows irregular three dimensional porous substrate of aluminum foam with submillimeter-scaled macro pores. In Fig. 1C and D, SEM image in large magnitude suggests the formation of a uniform layer structure which consisted of well-developed and thin plate-shaped crystals [26]. The layers structure was uniformly dispersed on the alumina foam surface. The tiny pores appear on the layer structure is further zoomed at high magnification as the image shown in Fig. 1E, and a hierarchically porous structure was probably obtained [27]. In addition, the layer structure shows a good durability after reaction and clearly remain on the aluminum surface (Fig. 1F). From EDS images in Fig. 3B–D, all elements, Cu, Zn, and Al, have a uniform distribution in the layer structure in Fig. 3A.

There is a clear capillary condensation step at the P/P<sub>0</sub> section of 0.4–0.6 in Fig. 4, which shows the meso-porous property of the calcined monolithic catalysts. According to the BJH model, the main meso pore diameter was 3.47 nm calculated from the nitrogen isotherms

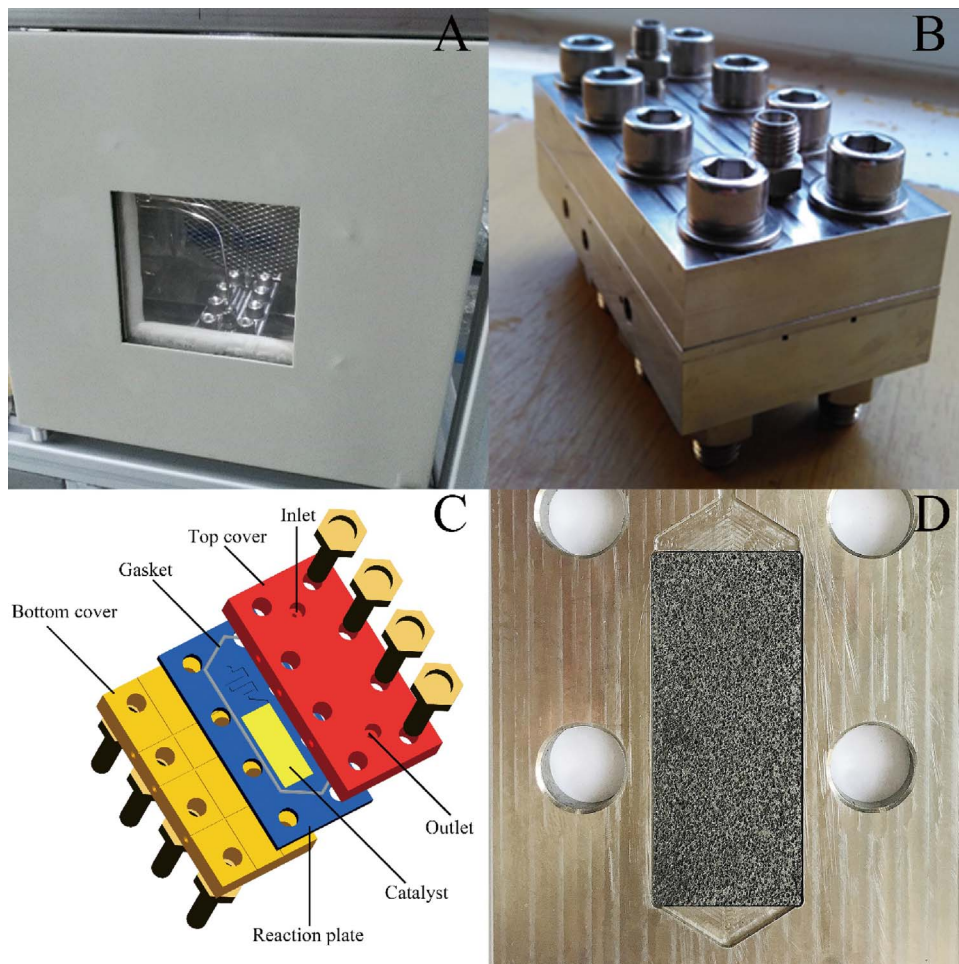


**Fig. 2.** A: the picture of microreactor in platform, B: outside view of microreactor, C: exploded view of microreactor, and D: screenshots of catalyst in chamber.

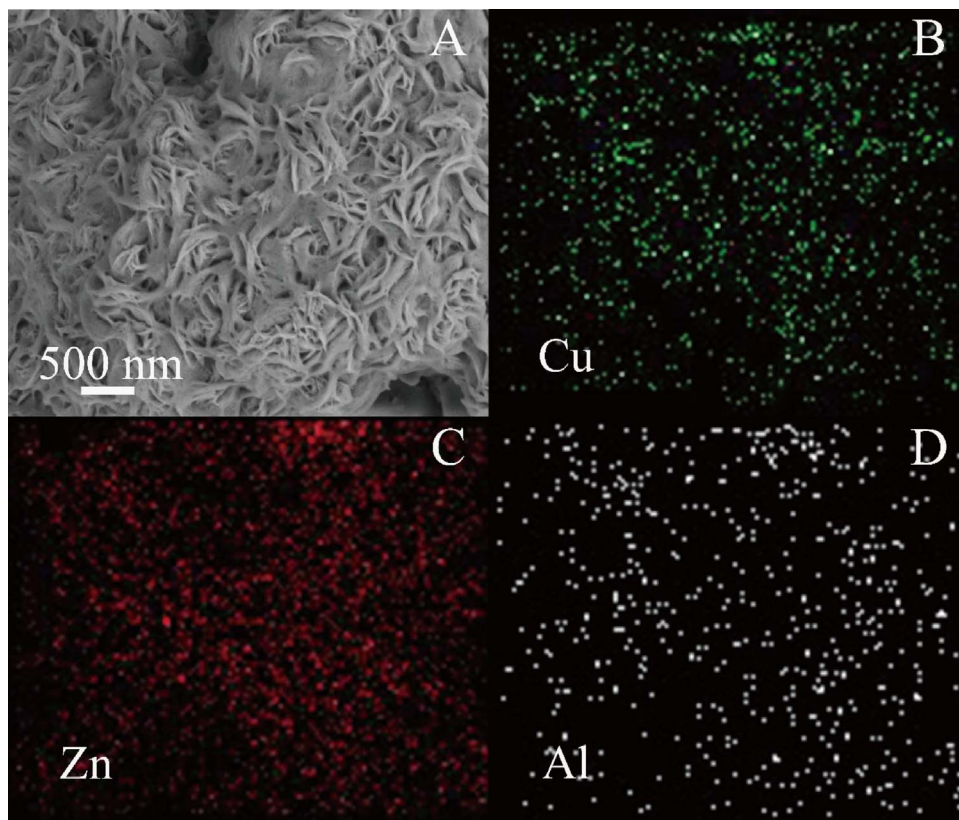


**Fig. 3.** A is the image of layer structure. B, C, D are the images of EDS and mapping results of the Cu, Zn and Al.

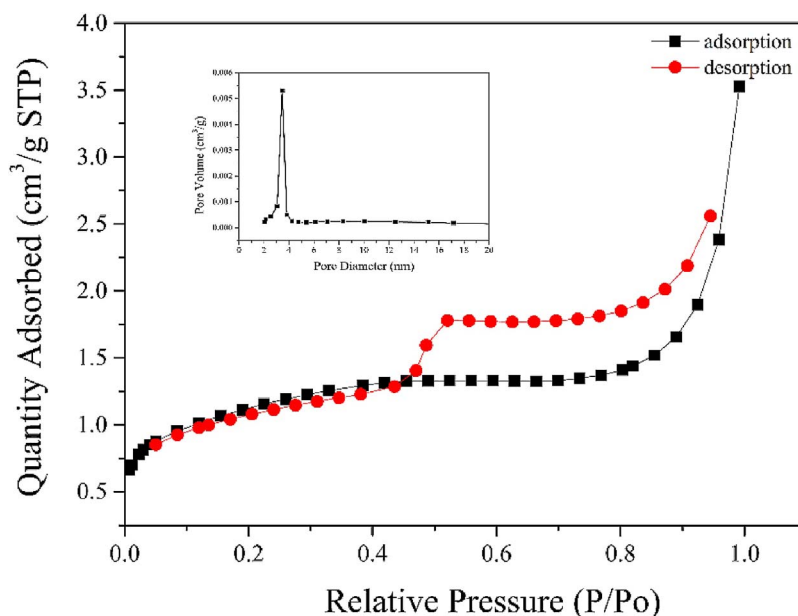


**Fig. 4.** Nitrogen adsorption-desorption isotherms and the BJH pore size distributions (inset) of the Cu-Zn/Al foam.

adsorption curve inserted in the chart. The specific surface area of pure aluminum foam was  $3.2 \text{ m}^2 \text{ g}^{-1}$  and it was increased to  $3.9 \text{ m}^2 \text{ g}^{-1}$  for Cu-Zn/Al foam, which might be attributed to high dispersion of layered particles anchored on the aluminum foam after treatment. The data of BET test was lower than normal particle catalyst because the sample was tested in a whole piece rather than grinded into powder, with the aim to explore the nature state of monolithic catalysts. Excluding the mass of aluminum foam, the layer structure contributes to the specific surface area and pore volume are  $30.4 \text{ m}^2 \text{ g}^{-1}$  and  $0.55 \text{ cm}^3 \text{ g}^{-1}$ , respectively.

The actual metal composition loaded on the foam was revealed by the ICP test in Table 1. The mole ratio of copper content in the monolithic catalyst was 2.07, and the ratio on the surface measured by XPS was 2.00. Those two values were in consistent with nominal compositions (2:1) set for the catalysts preparations, suggesting the complete precipitation of the metallic salts.

As shown in Fig. 5, the Cu-Zn/Al foam catalyst was detected by XRD. The pattern clearly indicated the diffraction peaks of catalyst were responding to the copper oxide (JCPDS-48-1548). This result solidly indicated that the copper has successfully united with alumina substrate. The diffraction peaks centered at  $2\theta$  of  $38.47^\circ$ ,  $44.74^\circ$ ,  $78.22^\circ$ ,  $82.44^\circ$  were attributed to aluminum (JCPDS-04-0787). And no obvious peaks of ZnO and Al<sub>2</sub>O<sub>3</sub> may be attributed to poor crystallinity, the amorphous state, or highly dispersed state [11,28–30].

The result of XPS in Fig. 6 proves the existence of Cu and Zn on the surface of foam. The binding energy peak of Cu 2p<sub>3/2</sub> was at 932.4 eV. Two strong satellite peaks of Cu<sup>2+</sup> were located at about 942.5 eV and 962.5 eV. In Fig. 6B, binding energy peak of Zn 2p<sub>3/2</sub> was at 1021.6 eV. Depending on the spectra, it indicates that the Cu and Zn were both at

**Table 1**  
Textural and structural properties of the Cu-Zn/Al foam monolithic catalyst.

Specific surface area ( $\text{m}^2 \text{ g}^{-1}$ ) <sup>a</sup>		Metal composition (wt %) <sup>b</sup>			Cu/Zn mole ratio on the surface <sup>c</sup>
Cu-Zn/ Al foam	LS contribution <sup>d</sup>	Cu	Zn	Cu/Zn mole ratio	
3.9	3.2	9.51	4.70	2.07	2.00

<sup>a,b,c</sup> Values measured by N<sub>2</sub>-BET, ICP, XPS respectively.

<sup>d</sup>Values defined as specific surface area of layer structure (LS) and calculated by BET method not including the mass of aluminum foam.

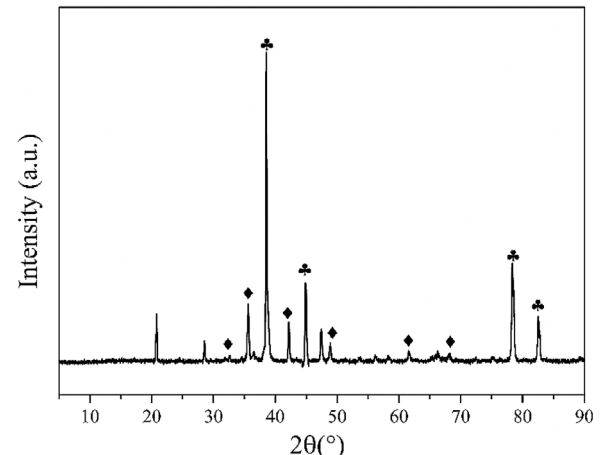


**Fig. 5.** The XRD pattern of calcined Cu-Zn/Al foam catalyst. CuO (◆), Al (●).

+2 oxidation states. The mass ratio of Cu and Zn was approximately 2:1 which is agreed with data of ICP, implying that Cu and Zn were uniformly loaded at the inside and outside of the foam.

### 3.1.2. The reducibility and basicity of catalysts

The H<sub>2</sub>-TPR spectra shows one consecutive peak of the monolithic catalysts in Fig. 7A. With a broad shoulder, a reduction peak can be observed within the range of 150–300 °C. According to the results of TPR measurements, the profiles were deconvoluted into two Gaussian peaks, low reduction peak (peak  $\alpha$ ) and high reduction peak (peak  $\beta$ ), implying the process of two steps copper species reduction. The intermediate, Cu<sub>2</sub>O, formed during the reduction [31].

The copper component was separated from layer structure firstly, and then individual Cu<sub>2</sub>O component was reduced by H<sub>2</sub>, which also confirmed that copper was the component of layer structure. Moreover, at the heating rate of  $10 \text{ }^\circ\text{C min}^{-1}$ , the reduction peak of the monolithic catalysts was about  $60 \text{ }^\circ\text{C}$  lower than the data of literature [32], suggesting much higher dispersion of copper species [33]. The area ratio of two peaks is about 2, which could be attributed to different types of copper, including highly dispersed and bulk copper [34]. The whole reduction temperature was lower than other copper based catalyst, which can be attributed to the high Cu dispersion and high heat transfer ability of the present catalyst [35,36].

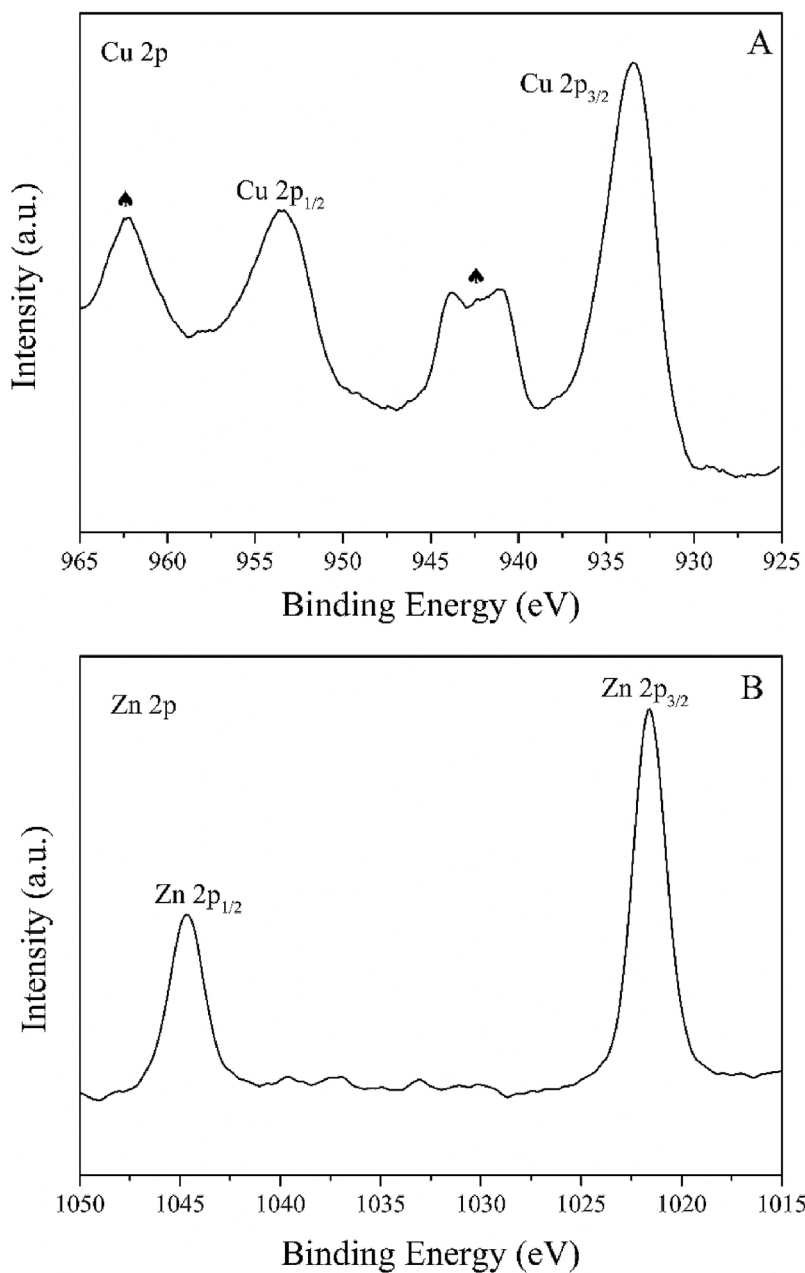


**Fig. 6.** The Cu 2p (A) and Zn 2p (B) spectra of the calcined Cu-Zn/Al foam catalyst. The symbol ( $\blacktriangle$ ) stand for satellite peak of  $\text{Cu}^{2+}$ .

The basicity of catalysts was measured by CO<sub>2</sub> temperature programmed desorption (CO<sub>2</sub>-TPD) and result is illustrated in Fig. 7B. A broad desorption peak appeared in the range of 50–200 °C. It is obvious that there is a high concentration of surface basic sites in the pre-reduced catalysts [33,37]. The detail data of different basic sites are given in Fig. 7B. The weakly basic site, denoted as  $\alpha$ , is related to OH<sup>−</sup> group, and the moderately basic site, denoted as  $\beta$ , is assigned to metal-oxygen pairs [7]. The strongly basic site, denoted as  $\gamma$ , appearing at 188 °C, is assigned to unsaturated O<sup>2−</sup> anions. The strongly basic site has been reported as a site of methanol synthesis mechanism so that it has a significant impact on the selectivity of CH<sub>3</sub>OH for CO<sub>2</sub> hydrogenation to methanol [38]. Some researchers have proposed that both methanol and CO are produced dominantly via the same reactive intermediates [12]. The 19.4% contribution of strongly basic sites is a suitable ratio for high methanol selectivity catalyst [39]. In addition, the formation of unsaturated O<sup>2−</sup> anions is related to the movement and partial decomposition of metal-oxygen pairs [40]. Compared with particle catalyst, the weakly basic sites in monolithic catalyst is increased, due to the larger amount of Al<sub>2</sub>O<sub>3</sub> in alumina foam which can enhance the weakly

basic sites [36].

### 3.2. Catalytic performance

#### 3.2.1. The effects of heat and mass transfer properties

The CO<sub>2</sub> hydrogenation to methanol is an exothermic reaction and the major side reaction is reverse water-gas shift that is endothermic. Enhancing the heat transfer ability of the reactor can efficiently improve the reaction of CO<sub>2</sub> hydrogenation to methanol and suppress the reaction of reverse water-gas shift. In this study, the porous aluminum foam substrate has excellent heat conductivity. The monolithic catalyst does not alter the nature of reaction and keeps the temperature distribution more uniformly hence effectively limit the hot spot [11,41]. It has been proved by Hutter et al. that metal foam can enhance the heat transfer in a large range of Reynolds numbers (600–7600) [42]. Thus, potent heat transfer property of monolithic catalyst is significant to prevent the formation of the hotspot that accelerates catalyst deactivation and reduce the selectivity of methanol. Meanwhile, mass transfer limitation in monolithic catalyst is discussed in Supplementary

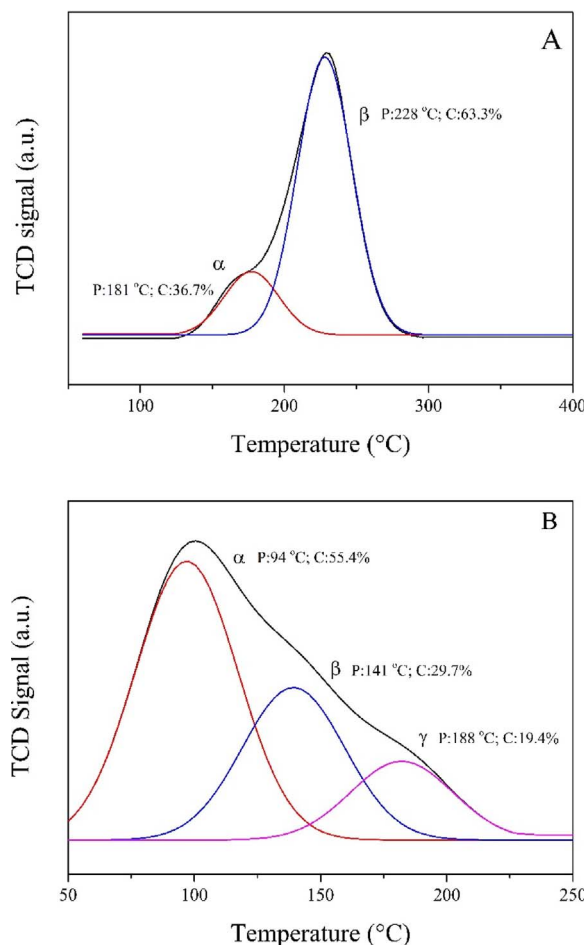


**Fig. 7.** (A) H<sub>2</sub>-TPR and (B) CO<sub>2</sub>-TPD profiles for Cu-Zn/Al foam catalyst (P: Position; C: Contribution).

material, which demonstrates that the reactions in this study are not controlled by external diffusion. Moreover, three dimensional porous aluminum foam can keep an extremely low pressure drop under high gas flow rate. The thickness of layer structure obtained in present work is below 10 μm which is far less than 50 μm and it has been reported as a threshold layer thickness causing diffusion limitations [43]. The catalytic data presented in this study are not affected by mass transport and the monolithic catalyst shows a good property of mass transfer. Compared with the literature, Cu-Zn/Al foam monolithic catalyst shows a good catalytic performance. A comparison of copper time yield of methanol is made among the present value (4.19 g g<sub>Cu</sub><sup>-1</sup> h<sup>-1</sup>) and other yields using different catalysts under the similar reaction conditions of 3 MPa, 250 °C, 10,000 mL g<sub>cat</sub><sup>-1</sup> h<sup>-1</sup>. The detail data are listed

**Table 2**  
Comparison of catalyst performance under similar reaction condition.

Catalyst	Reaction condition	Conversion of CO <sub>2</sub> (%)	CH <sub>3</sub> OH Selectivity (%)	CH <sub>3</sub> OH Yield <sup>a</sup> (g g <sub>Cu</sub> <sup>-1</sup> h <sup>-1</sup> )	Surface area (m <sup>2</sup> g <sup>-1</sup> )	Cu Dispersions
Cu-ZnO [33]	GHSV = 18,000 h <sup>-1</sup> , T = 250 °C, P = 3 MPa	4.1	35.1	0.11	N/A	3.4
Ga3.0-Cu-ZnO-ZrO <sub>2</sub> [44]	WHSV = 15,000 mL g <sub>cat</sub> <sup>-1</sup> h <sup>-1</sup> , T = 250 °C, P = 7 MPa	18	61	1.28	102	N/A
30CuZn-ZpH [45]	GHSV = 10,000 h <sup>-1</sup> , T = 260 °C, P = 5 MPa	19.6	50	1.51	79	N/A
Cu/ZnO-Al <sub>2</sub> O <sub>3</sub> [46]	GHSV = 10,471 h <sup>-1</sup> , T = 255 °C, P = 3 MPa	22.5	38.9	3.26	125	N/A
Cu-Zn/Al foam <sup>c</sup>	WHSV = 10,000 mL g <sub>cat</sub> <sup>-1</sup> h <sup>-1</sup> , T = 250 °C, P = 3 MPa	13.6	64.5	4.19	30.4	4.9 <sup>b</sup>

<sup>a</sup> The data are calculated by Eq. (6) if they were not directly provided in the reference paper.

<sup>b</sup> The data are calculated by Eq. (1).

<sup>c</sup> At the present work.

**Table 3**  
The result of evaluation test varied with temperature.

Reaction Temperature (°C)	Conversion of CO <sub>2</sub> (%)	CH <sub>3</sub> OH Selectivity (%)	CO Selectivity (%)	CH <sub>3</sub> OH Yield (g g <sub>Cu</sub> <sup>-1</sup> h <sup>-1</sup> )
220	9.2	78.1	21.9	3.42
230	9.9	76.0	24.0	3.59
240	9.9	66.5	33.5	3.15
250	13.6	64.5	35.4	4.19
260	15.5	50.6	49.4	3.75

Reaction conditions: Pressure = 3 MPa, WHSV = 10,000 mL g<sub>cat</sub><sup>-1</sup> h<sup>-1</sup>, H<sub>2</sub>/CO<sub>2</sub>/N<sub>2</sub> = 73/24/3 (molar ratio).

in Table 2. The high CH<sub>3</sub>OH selectivity and yield have been achieved though the specific surface area and Cu dispersion of monolithic catalyst do not show a significant advantage. It is speculated that the advance heat and mass transfer properties of the microreactor result in the high methanol selectivity of Cu-Zn/Al foam catalyst.

### 3.2.2. The effects of reaction conditions

A parametric study was also carried out to investigate the effect of reaction conditions on CO<sub>2</sub> hydrogenation to methanol system. The synthesis of methanol (Eq. (2)) and the reverse water gas shift (RWGS) (Eq. (3)) are both thermodynamically limited reactions [35,44,47]. The influence of reaction temperature, pressure and space velocity on catalytic performance of CO<sub>2</sub> hydrogenation in microreactor are summarized in Tables 3–5, respectively.

Table 3 indicates that with the rising of reaction temperature from 220 to 260 °C, the CO<sub>2</sub> conversion and the formation of CO are both gradually promoted. This phenomena is consistent with the system using particle catalyst [39]. The CO<sub>2</sub> conversion gradually approaches to equilibrium with increasing reaction temperature, which indicates that CO<sub>2</sub> conversion could be improved kinetically with the temperature rising from 220 °C to 260 °C [7]. The variation tendency of methanol selectivity is consistent with the result obtained at thermodynamic equilibrium as given in Fig. S2. The optimum operating temperature is suggested to be 250 °C in order to obtain a maximum methanol yield that is affected synthetically by CO<sub>2</sub> conversion and methanol selectivity. In this case, the copper time yield of methanol is 4.19 g g<sub>Cu</sub><sup>-1</sup> h<sup>-1</sup>.

As shown in Table 4, increasing the reaction pressure from 2 MPa to 5 MPa, the conversion rate of CO<sub>2</sub> grows. This trend is consistent with principle of Le Chatelier in which the equilibrium moves toward volume contraction and the synthesis of methanol (Eq. (2)) prevails. The maximum yield of methanol is 7.33 g g<sub>Cu</sub><sup>-1</sup> h<sup>-1</sup> at 19.7% CO<sub>2</sub> conversion and 77.9% selectivity to methanol, under the condition of 250 °C, 5 MPa, 10,000 mL g<sub>cat</sub><sup>-1</sup> h<sup>-1</sup>. Nevertheless, a high reaction pressure demands a higher standards of both reactor and platform, with potential safety problem.

The performance of catalyst with the change of WHSV is

**Table 4**

The result of evaluation test varied with pressure.

Pressure (MPa)	Conversion of CO <sub>2</sub> (%)	CH <sub>3</sub> OH Selectivity (%)	CO Selectivity (%)	CH <sub>3</sub> OH Yield (g g <sub>cat</sub> <sup>-1</sup> h <sup>-1</sup> )
2	12.1	45.4	54.6	2.63
3	13.6	64.5	35.5	4.19
4	16.6	76.2	23.8	6.05
5	19.7	77.9	22.0	7.33

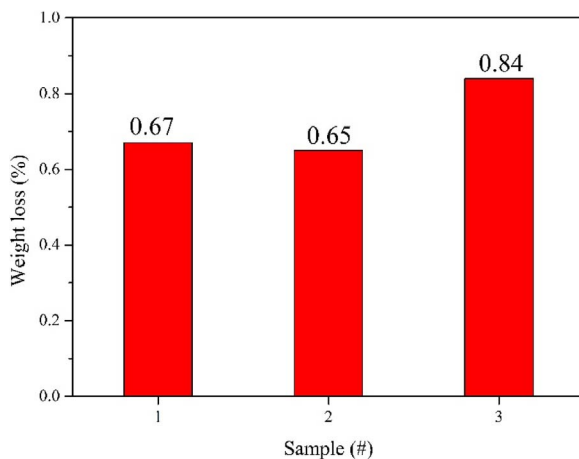
Reaction conditions: Temperature = 250 °C, WHSV = 10,000 mL g<sub>cat</sub><sup>-1</sup> h<sup>-1</sup>, H<sub>2</sub>/CO<sub>2</sub>/N<sub>2</sub> = 73/24/3 (molar ratio).

**Table 5**

The result of evaluation test varied with WHSV.

WHSV (mL g <sub>cat</sub> <sup>-1</sup> h <sup>-1</sup> )	Conversion of CO <sub>2</sub> (%)	CH <sub>3</sub> OH Selectivity (%)	CO Selectivity (%)	CH <sub>3</sub> OH Yield (g g <sub>cat</sub> <sup>-1</sup> h <sup>-1</sup> )
5000	15.1	46.4	53.6	1.68
10000	13.6	64.4	35.5	4.19
15000	11.0	72.7	27.3	5.76
20000	9.9	82.7	17.3	7.81

Reaction conditions: Pressure = 3 MPa, Temperature = 250 °C, H<sub>2</sub>/CO<sub>2</sub>/N<sub>2</sub> = 73/24/3 (molar ratio).

**Fig. 8.** Weight loss of adhesion test for three samples in this study.

summarized in **Table 5**. The high weight hourly space velocity (WHSV) used in microreactor can significantly increase the selectivity of methanol [48,49]. From 5000 to 20,000 mL g<sub>cat</sub><sup>-1</sup> h<sup>-1</sup>, the conversion of CO<sub>2</sub> decreases from 15.1% to 9.9% while the selectivity of methanol increases from 46.4% to 82.7%. According to thermodynamic analysis in Fig. S2, the methanol selectivity (46.4%) at 5000 mL g<sub>cat</sub><sup>-1</sup> h<sup>-1</sup> is close to methanol selectivity (47.0%) at equilibrium of 250 °C, 3 MPa [35]. Generally, with the growth of WHSV, methanol formation rate has a linear increase while the formation rate of side product, CO, is easy to reach equilibrium point to make the ratio of methanol to CO larger [50]. The variation tendency of methanol selectivity is in consistent with the literature [51].

### 3.3. The practicality of catalyst

The monolithic catalyst and microreactor have been developed to enhance heat and mass transfer in the reaction system. The replacement and adhesion are significant in practicality in microreactor. Compared with present methods, the monolithic catalyst is more convenient in the replacement of spent catalysts, as other methods are often difficult in changing the spent washcoating layer or catalyst particles in

microchannel [52]. The adhesion test of layer structure on aluminum foam was performed in an ultrasonic vibrating instrument (JP-031S, Skymen Cleaning Equipment Shenzhen Co., Ltd) [53]. The result of adhesion test is shown in **Fig. 8** and weight loss of 1#, 2#, 3# sample are 0.67%, 0.65%, 0.84%, respectively. The average value, only 0.7%, indicates a good adhesion property of our monolithic catalyst. Generally, with the good practicality and property, the monolithic catalyst in microreactor has a great potential to intensify the reaction process.

## 4. Conclusions

A novel preparation method was developed for monolithic catalyst integrated with microreactor to perform CO<sub>2</sub> hydrogenation to methanol, i.e. highly porous hydroxides films in three dimension were synthesized on aluminum foam under the near-neutral pH at the ambient temperature. Such a route not only avoid the problem of wash-coating layer which is often easily cracked, but also give rise to the catalyst of a greater heat and mass transfer properties. Compared with other copper based catalyst in properties, Cn-Zn/Al foam catalyst possess a good heat/mass transfer ability and suitable ratio of strongly basic site. Nevertheless, the monolithic catalyst do not show superiorities in some properties including specific surface area and Cu dispersion. The catalyst delivers a high yield of methanol of 7.81 g g<sub>Cu</sub><sup>-1</sup> h<sup>-1</sup> at CO<sub>2</sub> conversion of 9.9% and methanol selectivity of 82.7% under condition of 3 MPa and 250 °C at a high WHSV of 20,000 mL g<sub>cat</sub><sup>-1</sup> h<sup>-1</sup> in a microreactor, providing an innovative solution for exothermic reactions. Comprehensively speaking, the combination of monolithic catalysts with microreactor could intensify the process and achieve an outstanding result.

## Acknowledgements

This work was financially supported by the Global Innovation Initiative: Increasing the efficiency of CO<sub>2</sub> conversion to liquid fuels (S-ECAGD-13-CA-149(DT)) and Shanghai Municipal Science and Technology Commission, China (16DZ1206900).

## Appendix A. Supplementary data

Supplementary data associated with this article can be found, in the online version, at <http://dx.doi.org/10.1016/j.jcou.2017.05.023>.

## Reference:

- [1] K.A. Carrado, J.H. Kim, C.S. Song, N. Castagnola, C.L. Marshall, M.M. Schwartz, Catal. Today 116 (4) (2006) 478–484.
- [2] K.D. Ramachandriya, D.K. Kundiyana, M.R. Wilkins, J.B. Terrill, H.K. Atiyeh, R.L. Huhneke, Appl. Energy 112 (2013) 289–299.
- [3] G. Centi, G. Giordano, P. Fejes, A. Katovic, K. Lazar, J.B. Nagy, S. Perathoner, Studies in Surface Science and Catalysis, Elsevier, 2004, pp. 2566–2573.
- [4] G.A. Olah, A. Goeppert, G.K. Prakash, J. Org. Chem. 74 (2) (2009) 487–498.
- [5] M. Sahibzada, I.S. Metcalfe, D. Chadwick, J. Catal. 174 (2) (1998) 111–118.
- [6] J.A. Rodriguez, P. Liu, D.J. Stacciola, S.D. Senanayake, M.G. White, J.G.G. Chen, ACS Catal. 5 (11) (2015) 6696–6706.
- [7] X. Dong, F. Li, N. Zhao, F. Xiao, J. Wang, Y. Tan, Appl. Catal. B: Environ. 191 (2016) 8–17.
- [8] T. Inui, T. Takeguchi, Catal. Today 10 (1) (1991) 95–106.
- [9] Y. Liu, D. Edouard, L.D. Nguyen, D. Begin, P. Nguyen, C. Pham, C. Pham-Huu, Chem. Eng. J. 222 (2013) 265–273.
- [10] L.P. Han, C.Z. Wang, G.F. Zhao, Y. Liu, Y. Lu, AIChE J. 62 (3) (2016) 742–752.
- [11] Y.K. Li, Q.F. Zhang, R.J. Chai, G.F. Zhao, Y. Liu, Y. Lu, F.H. Cao, AIChE J. 61 (12) (2015) 4323–4331.
- [12] P. Gao, F. Li, H. Zhan, N. Zhao, F. Xiao, W. Wei, L. Zhong, H. Wang, Y. Sun, J. Catal. 298 (2013) 51–60.
- [13] M. Lenarda, E. Moretti, L. Storaro, P. Patrono, F. Pinzari, E. Rodríguez-Castellón, A. Jiménez-López, G. Busca, E. Finocchio, T. Montanari, R. Frattini, Appl. Catal. A: Gen. 312 (2006) 220–228.
- [14] L.H. Zhang, C. Zheng, F. Li, D.G. Evans, X. Duan, J. Mater. Sci. 43 (1) (2008) 237–243.
- [15] H. Wang, P. Gao, T.J. Zhao, W. Wei, Y.H. Sun, Sci. China Chem. 58 (1) (2015) 79–92.
- [16] P. Gao, R. Xie, H. Wang, L. Zhong, L. Xia, Z. Zhang, W. Wei, Y. Sun, J. CO<sub>2</sub> Util. 11

- (2015) 41–48.
- [17] P. Gao, F. Li, F.K. Xiao, N. Zhao, N.N. Sun, W. Wei, L.S. Zhong, Y.H. Sun, *Catal. Sci. Technol.* 2 (7) (2012) 1447–1454.
- [18] L.C. Almeida, F.J. Echave, O. Sanz, M.A. Centeno, G. Arzamendi, L.M. Gandía, E.F. Sousa-Aguiar, J.A. Odriozola, M. Montes, *Chem. Eng. J.* 167 (2–3) (2011) 536–544.
- [19] L.F. Bobadilla, A. Álvarez, M.I. Domínguez, F. Romero-Sarria, M.A. Centeno, M. Montes, J.A. Odriozola, *Appl. Catal. B: Environ.* 123–124 (2012) 379–390.
- [20] S. Koc, A.K. Avci, *Fuel Process. Technol.* 156 (2017) 357–365.
- [21] K.F. Jensen, *Chem. Eng. Sci.* 56 (2) (2001) 293–303.
- [22] N. Al-Rifai, E.H. Cao, V. Dua, A. Gavrilidis, *Curr. Opin. Chem. Eng.* 2 (3) (2013) 338–345.
- [23] C.D. Wagner, L.E. Davis, M.V. Zeller, J.A. Taylor, R.H. Raymond, L.H. Gale, *Surf. Interface Anal.* 3 (5) (1981) 211–225.
- [24] P. Gao, F. Li, N. Zhao, F.K. Xiao, W. Wei, L.S. Zhong, Y.H. Sun, *Appl. Catal. A-Gen.* 468 (2013) 442–452.
- [25] N. Bette, J. Thielemann, M. Schreiner, F. Mertens, *ChemCatChem* 8 (18) (2016) 2903–2906.
- [26] Z. Ni, A. Chen, C. Fang, L. Wang, W. Yu, *J. Phys. Chem. Solids* 70 (3–4) (2009) 632–638.
- [27] W.K. Jo, J.Y. Lee, T.S. Natarajan, *Phys. Chem. Chem. Phys.* 18 (2) (2016) 1000–1016.
- [28] J. Cheng, J.J. Yu, X.P. Wang, L.D. Li, J.J. Li, Z.P. Hao, *Energy Fuel* 22 (4) (2008) 2131–2137.
- [29] M. Behrens, I. Kasatkin, S. Kuhl, G. Weinberg, *Chem. Mater.* 22 (2) (2010) 386–397.
- [30] H.M.T. Galvis, J.H. Bitter, C.B. Khare, M. Ruitenbeek, A.I. Dugulan, K.P. de Jong, *Science* 335 (6070) (2012) 835–838.
- [31] S. Xiao, Y. Zhang, P. Gao, L. Zhong, X. Li, Z. Zhang, H. Wang, W. Wei, Y. Sun, *Catal. Today* 281 (Part 2) (2017) 327–336.
- [32] S. Kuhl, A. Tarasov, S. Zander, I. Kasatkin, M. Behrens, *Chem.-Eur. J.* 20 (13) (2014) 3782–3792.
- [33] C. Tisseraud, C. Comminges, T. Belin, H. Ahouari, A. Soualah, Y. Pouilloux, A. Le Valant, *J. Catal.* 330 (2015) 533–544.
- [34] I. Ud Din, M.S. Shaharun, D. Subbarao, A. Naeem, *J. Power Sources* 274 (2015) 619–628.
- [35] H. Yang, P. Gao, C. Zhang, L. Zhong, X. Li, S. Wang, H. Wang, W. Wei, Y. Sun, *Catal. Commun.* 84 (2016) 56–60.
- [36] Y. Zhang, L. Zhong, H. Wang, P. Gao, X. Li, S. Xiao, G. Ding, W. Wei, Y. Sun, *J. CO<sub>2</sub> Util.* 15 (2016) 72–82.
- [37] Y. Liu, K. Sun, H. Ma, X. Xu, X. Wang, *Catal. Commun.* 11 (10) (2010) 880–883.
- [38] P. Gao, F. Li, H. Zhan, N. Zhao, F. Xiao, W. Wei, L. Zhong, Y. Sun, *Catal. Commun.* 50 (2014) 78–82.
- [39] C. Zhang, H. Yang, P. Gao, H. Zhu, L. Zhong, H. Wang, W. Wei, Y. Sun, *J. CO<sub>2</sub> Util.* 17 (2017) 263–272.
- [40] G.D. Wu, X.L. Wang, W. Wei, Y.H. Sun, *Appl. Catal. A-Gen.* 377 (1–2) (2010) 107–113.
- [41] C.G. Visconti, G. Groppi, E. Tronconi, *Catal. Today* 273 (2016) 178–186.
- [42] C. Hutter, D. Büchi, V. Zuber, P. Rudolf von Rohr, *Chem. Eng. Sci.* 66 (17) (2011) 3806–3814.
- [43] E. Iglesia, S.C. Reyes, R.J. Madon, S.L. Soled, *Advances in Catalysis*, Academic Press, 1993, pp. 221–302.
- [44] R. Ladera, F.J. Pérez-Alonso, J.M. González-Carballo, M. Ojeda, S. Rojas, J.L.G. Fierro, *Appl. Catal. B: Environ.* 142–143 (2013) 241–248.
- [45] L. Angelo, M. Girleanu, O. Ersen, C. Serra, K. Parkhomenko, A.-C. Roger, *Catal. Today* 270 (2016) 59–67.
- [46] A. Bansode, A. Urakawa, *J. Catal.* 309 (2014) 66–70.
- [47] S. Saeidi, N.A.S. Amin, M.R. Rahimpour, *J. CO<sub>2</sub> Util.* 5 (2014) 66–81.
- [48] Y. Zhang, J. Fei, Y. Yu, X. Zheng, *Energy Convers. Manage.* 47 (18–19) (2006) 3360–3367.
- [49] Y.P. Zhang, J.H. Fei, Y.M. Yu, X.M. Zheng, *J. Nat. Gas Chem.* 16 (1) (2007) 12–15.
- [50] C. Li, X. Yuan, K. Fujimoto, *Appl. Catal. A: Gen.* 469 (2014) 306–311.
- [51] F. Arena, G. Mezzatesta, G. Zafarana, G. Trunfio, F. Frusteri, L. Spadaro, *J. Catal.* 300 (2013) 141–151.
- [52] L.C. Almeida, F.J. Echave, O. Sanz, M.A. Centeno, J.A. Odriozola, M. Montes, *Stud. Surf. Sci. Catal.* 175 (2010) 25–33.
- [53] X. Ying, L. Zhang, H. Xu, Y.-L. Ren, Q. Luo, H.-W. Zhu, H. Qu, J. Xuan, *Fuel Process. Technol.* 143 (2016) 51–59.